JOURNAL OF APPLIED ELECTROCHEMISTRY 11 (1981) 91–102

Heat rejection and thermal efficiency in model hydrogen–halogen fuel cell systems

E. N. BALKO

General Electric Company, Direct Energy Conversion Programs, Wilmington, Massachusetts, USA

Received 18 March 1980

The efficiency and heat rejection characteristics of the H_2/Cl_2, H_2/Br_2 and H_2/I_2 fuel cell systems have been studied by computer simulation. The H_2/Cl_2 and H_2/Br_2 systems are comparable in terms of efficiency, heat rejection and fuel mass. The H_2/I_2 system is markedly less efficient.

1. Introduction

There has been increasing interest in recent years in hydrogen–halogen fuel cells as both primary and regenerative energy storage systems [1–3]. The attractiveness of the hydrogen–halogen systems lies in the high degree of reversibility characteristic of halogen electrodes; the potential for low-pressure storage of the halogen oxidant as a clathrate (in the case of chlorine) or in solution (in the cases of bromine and iodine); and the relatively high energy storage density possible with the lighter halogens.

A regenerative fuel cell system is, in reality, a secondary battery. In contrast to the oxygen–hydrogen fuel cell, the reaction product activity in a regenerative hydrogen–halogen fuel cell increases continuously throughout the discharge cycle. This change in activity causes a number of cell characteristics to change during discharge.

While fuel cells are free of the Carnot limitations on the conversion of chemical to electrical energy which exist for combustion processes, fuel cells are not completely efficient devices. The overall process in a hydrogen–halogen fuel cell

$$H_2 + X_2 = 2HX\,(aq)$$

results in the formation of a substance in the liquid phase from one or more gases. Consequently, the Gibbs free energy change for the process, and hence the cell potential, is less than the enthalpy change due to halogen acid formation. This energy difference appears as heat during the discharge of the fuel cell and is the single largest source of waste heat evolved during discharge of a practical hydrogen–halogen system. Due to the increasing change in reaction entropy, the quantity of waste heat evolved per mole of acid formed increases with acid concentration. Fig. 1 illustrates the increase in uncompensated heat of formation with acid concentration for the hydrogen–chlorine, hydrogen–bromine and hydrogen–iodine couples.

The absolute value of the waste heat generated in this way is greatest in the hydrogen–chlorine couple where the entropy change is largest. In an energy storage application, it is often the quantity of waste heat relative to the electrical energy recovered which is of consequence. Fig. 2 illustrates the decrease in cell voltage with increased acid concentration for each of the hydrogen–halogen couples. The data in Fig. 3 show the quantity of waste heat relative to the reversible electrical energy as a function of acid concentration for the three halogen acids. The relative amount of waste heat liberated is greatest for the hydrogen–iodine couple, where the small free energy change for HI formation amplifies the effect due to increasing entropy change.

The cell separator characteristics will also change as the halogen acid concentration increases. In cells which employ a microporous matrix or diaphragm, electrical current is carried by the electrolyte solution flooding the matrix porosity. The change in halogen acid resistivity with concentration is shown in Fig. 4. Those fuel cells which employ an ion-exchange polymer membrane as the cell separator also undergo a change in separator resistance with the halogen acid concentration. An ion-exchange material in contact with an aqueous electrolyte gives rise to a partitioning of water

0021–891X/81/010091–12$03.20/0

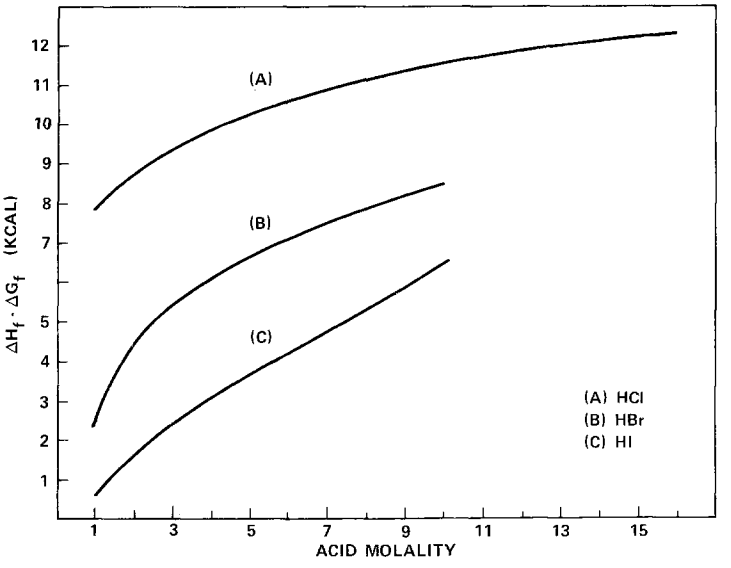

Fig. 1. Uncompensated heat of formation of the halogen acids at 25° C. Data from Reference [10].

across the phase boundary until the water activity is equal in both phases. The decreasing solvent activity with increasing halogen acid concentration dehydrates the membrane, as shown in Fig. 5. This causes the polymer phase resistivity to undergo the increase shown in Fig. 6.

The combined effects of decreasing output potential, increasing waste heat evolution and changing separator resistance can become significant in practical hydrogen–halogen regenerative energy-storage systems. Many applications of such power systems require the delivery of constant output power to an external load. As the cell potential decreases, an increasing quantity of fuel must be consumed in order to deliver the same quantity of electrical power. This, in turn, leads to the evolution of an increasing quantity of waste heat evolved per unit of electrical power delivered;

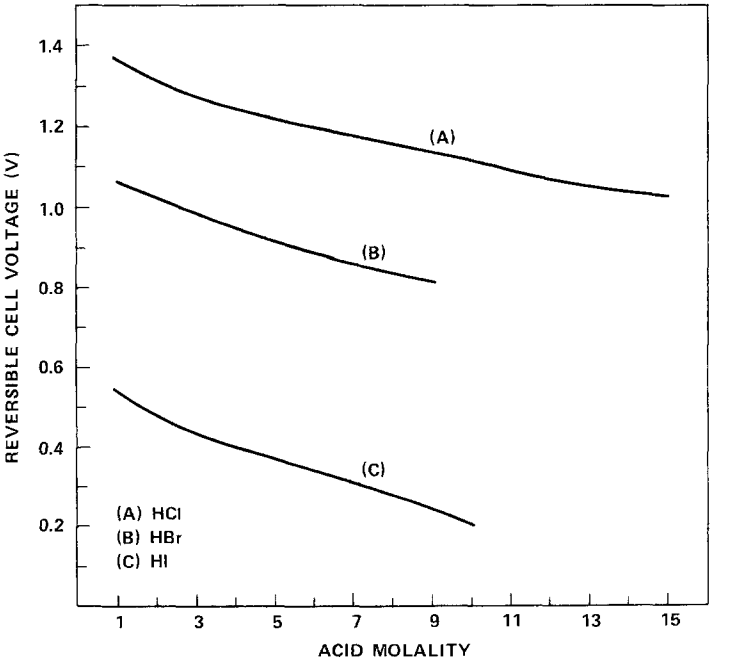

Fig. 2. Reversible potential of the cell: $Pt/H_2/HX/X_2/Pt$ at 25° C.

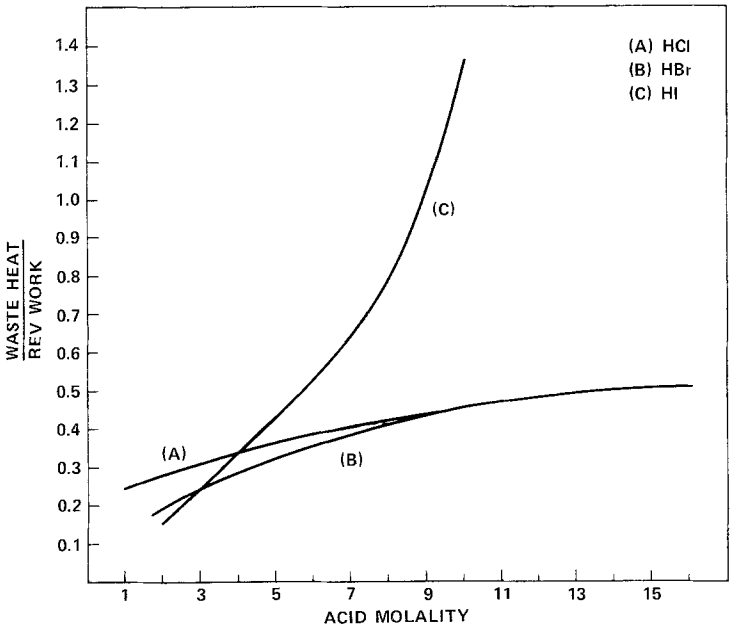

Fig. 3. Ratio of the uncompensated heat of formation to the reversible electrical energy output for the halogen acids at 25° C.

the increased cell current will cause the waste heat generated by polarization losses and separator resistance to increase in unison. The effect is compounded if the separator resistance is also increasing.

This paper considers the heat rejection, fuel requirements and efficiency of several model hydrogen–halogen fuel cell systems during the discharge cycle.

2. Computer simulation

Several numerical models of hydrogen–halogen fuel cells were constructed as part of this work. The primary restraint on the model was that it should deliver a constant output power to 10 kW for a 1500 kW h cycle. All systems were started from a halogen acid concentration of 1.4 molal. The fuel cell battery was operated isothermally at

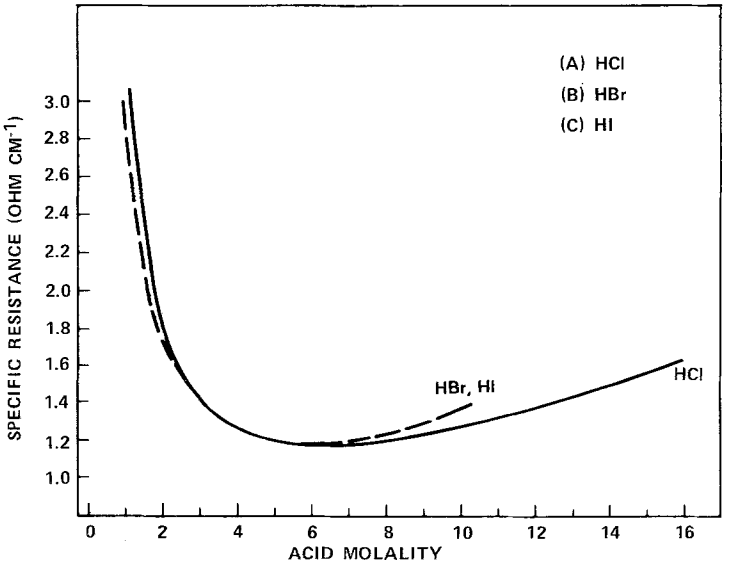

Fig. 4. Specific resistance of the halogen acids at 25° C. From the data of Reference [14].

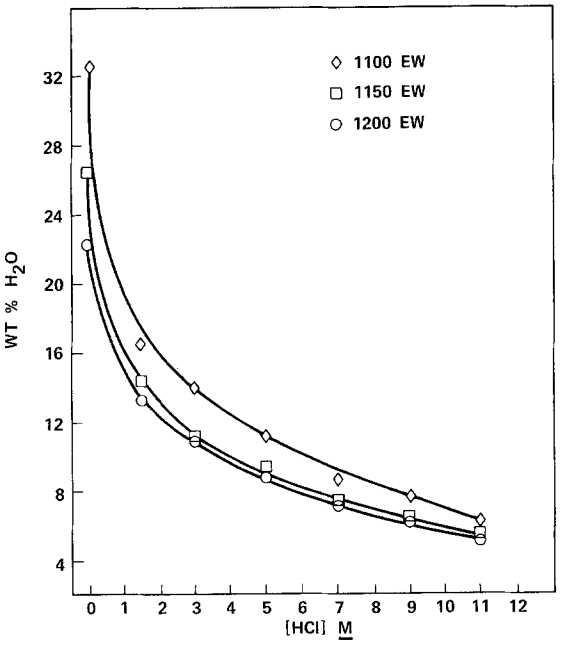

Fig. 5. Water content of Nafion sulphonic acid membranes at 25° C as a function of HCl molarity.

25° C; all heat evolved in the system was removed. Due to lack of data in the literature on the heat capacities of HBr and HI, particularly at the higher concentrations, no account was taken of changes in liquid heat content at 25° C. The heat capacity of aqueous HCl changes less than 2% over the concentration range of 2–17 molal when expressed on a constant water mass basis [4]. The change for the other halogen acids might be anticipated to be similarly small so the lack of correction for the change in heat capacity was felt to introduce negligible error. The fuel cell systems modelled had electrodes bonded directly to the cell separator. For this reason no consideration of ohmic losses in electrolyte gaps was necessary.

The reversible cell potential at 25° C and each

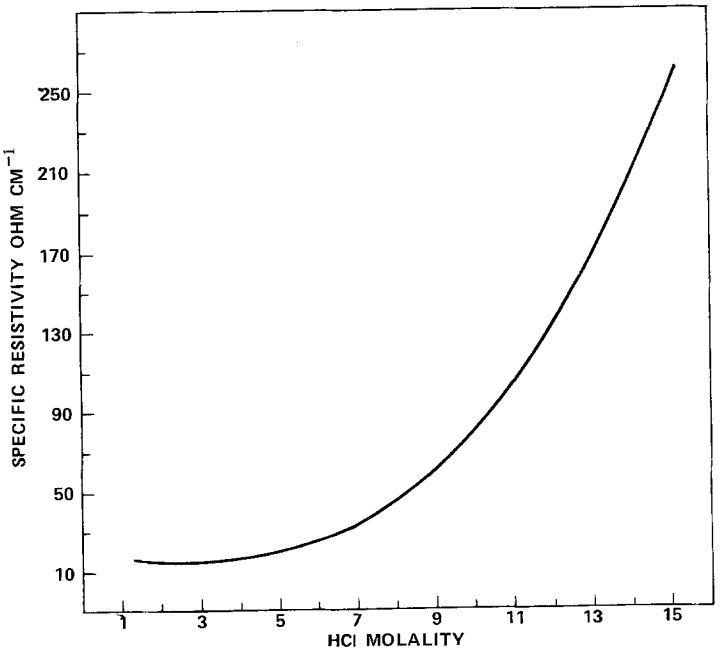

Fig. 6. The variation in resistance of Nafion 1200 EW polymer in equilibrium with aqueous HCl at 25° C. From the data of Reference [1].

Table 1. Activity coefficients of the halogen acids at 25° C

Acid molality	*log γ*		
	HCl	*HBr*	*HI*
1	−0.092	−0.055	−0.016
2	0.0039	0.073	0.132
3	0.119	0.229	0.304
4	0.246	0.400*	0.468*
5	0.376	0.565	0.640*
6	0.508	0.788	0.803
7	0.640	0.915	0.987
8	0.771	0.049	1.207
9	0.900	1.199	1.484
10	1.018	1.362	1.763
11	1.130	1.524	
12	1.236		
13	1.338		
14	1.436		
15	1.532		
16	1.627		
References	[5]	[6–8]	[8, 9]

* By extrapolation.

acid concentration was calculated from the Nernst equation

$$E_{cell} = E^0_{cell} + \frac{RT}{F} \ln (\gamma^2 C^2_{HX} / a^{1/2}_{H_2} a^{1/2}_X)$$

where C_{HX} is the acid molality and γ the activity coefficient. The acid activity coefficients listed in Table 1 were used. The chlorine activity was taken as equal to its partial pressure. The bromine and iodine activities were taken as unity; that is, the acid solution was assumed to be at saturation with its respective halogen. Enthalpy of formation data at different acid concentrations were taken from Reference [10]. The uncompensated heat of formation was calculated as the difference between the reversible cell potential, expressed as heat, and the enthalpy of formation at that concentration.

The total cell overpotential was described by a Tafel relationship

$$\eta = 0.05 + (0.06)\log i.$$

The slope and intercept are reasonable values for the common electrocatalysts used in halogen systems [11]. All polarization losses were taken to appear in the system as waste heat. The resistance R of the matrix separator was calculated as the resistance of the same thickness of liquid acid divided by the matrix porosity

$$R_{sep} = \frac{(\text{Specific resistance of HX at } C_{HX})(\text{Separator thickness})}{(\text{Separator porosity})}.$$

A matrix of 0.25 mm thickness with a porosity of 0.2 was modelled. These values are characteristic of at least one type of microporous cell separator [12, 13]. The acid concentration was assumed to be uniform across the matrix. Values of the halogen acid resistivities were calculated from the data of Reference [14].

For reasons not considered here, a matrix separator may not prove suitable for hydrogen–halogen applications. Diffusional losses, particularly with the bromine and iodine systems during charging and standby periods, may preclude the use of a microporous separator. Matrix systems are included in this work for completeness.

The ion-exchange membranes in solid polymer electrolyte systems were taken to be in equilibrium with the halogen acid. Nafion 1200 EW material in the form of a 0.1 mm film was modelled; this is a commercially available material and has been used in this application in our laboratory. No data are available on the resistance of Nafion in equilibrium with aqueous HBr or HI. The water activity in solutions of these acids, as manifested by the osmotic coefficients [9] and water vapour pressures [4], closely parallels that of the solvent in aqueous HCl. The approximation was therefore made that all three acids obeyed the resistance versus acid molality relationship described by Fig. 6.

The thermal efficiency, as used in this paper, is defined as

$$\text{Thermal efficiency} = \frac{(\text{Total delivered power in calories})}{(\text{Total moles HX formed})(\Delta H^0_{298})} \times 100\%$$

The model functioned by determining the reversible potential of the system at the start of the cycle and then calculating the current required to meet the constant power output requirement. With this value of the current, the internal polarization and ohmic losses were determined. A new value of the current was next calculated to deliver

the prescribed power with consideration for the internal losses. This, in turn, permitted the recalculation of the internal losses; the iterative process was continued until the system current at the effective output voltage delivered the required power to within 0.5%. This convergence would normally require 15 to 25 iterations. The system then operated at the convergence current for 120 s and a new value of the halogen acid molality was calculated on the basis of the current passed. The iterative process was then repeated to calculate a new system current corresponding to the changed cell conditions. This was continued for the entire 150 h cycle duration, with the model controlling the fuel consumption at whatever rate was necessary to meet the constant power output requirement.

In some cases, the effective output voltage went to zero due to large internal losses arising because of the fuel charge specified. In such cases the program was structured to terminate and to report the occurrence.

The simulation was, in effect, a numerical integration of the energy relationships which describe the system with a time increment dt of two minutes. The Honeywell L 64 timesharing system in our laboratory was used for the simulation.

3. The H_2/Cl_2 systems

A system which employs chlorine as a reactant has an inherent limitation imposed on the current density by the sparing solubility of chlorine in aqueous HCl [1, 15]. Recent work by J. McElroy in our laboratory has demonstrated that limiting current densities in excess of 350 mA cm^{-2} are attainable with suitably structured electrodes at 10 atm chlorine pressure [3]. The use of a matrix separator is doubtful at this pressure due to the very high bubble pressure necessary to prevent intercompartment mixing.

These considerations dictated the specific H_2/Cl_2 systems considered. The first case was a solid polymer electrolyte system of 9.45 m^2 at a chlorine pressure of 10 atm. The other cases considered were a solid polymer electrolyte and a matrix system of 37.8 m^2 (400 ft^2) operating at 1 atm chlorine pressure. The 9.45 m^2 system corresponded to a current density of ~ 100 mA cm^{-2} and the larger systems to a current density of ~ 25 mA cm^{-2}. The current density in the larger systems is well within the limits reported for 1 atm chlorine pressure [1].

Fig. 7 describes the change in several cell parameters as a function of time into the discharge

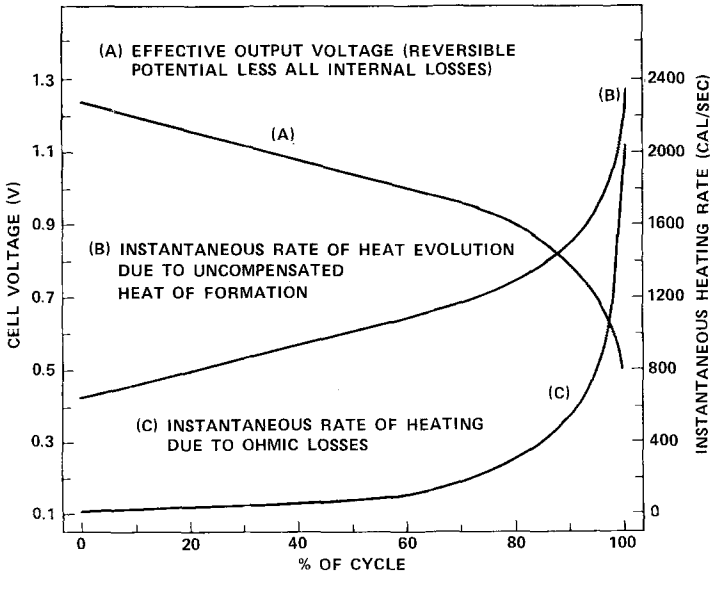

Fig. 7. Cell behaviour during the discharge of the SPE H_2/Cl_2, 94.5 m^2 system; 13.8 molal final HCl concentration.

cycle for the 9.45 m^2 system. The effective output voltage decreases nearly linearly for the first 70% of the cycle until the point is reached where the acid concentration is near 9 molal. At this concentration, the separator resistance is beginning to increase rapidly. This forces a higher current on the battery and produces the consequent rapid increase in internal losses and waste heat evolution for the duration of the cycle. When the fuel charge specified is such that the 9 molal concentation is not reached, system performance resembles that shown in Fig. 7 prior to the 70% discharge point. The effects are, of course, sensitive to current density and of lower magnitude in the larger-area batteries.

The overall thermal efficiency of the three cases considered is shown in Fig. 8 as a function of the final HCl concentration. The nonlinearity of the upper and lower curves is due to the rapid changes in separator resistance which occur at different concentrations for the solid polymer electrolyte and matrix systems. Fig. 9 shows the relationship between final HCl molality and the quantity of heat rejected during the cycle. The nonlinear behaviour in Fig. 8 is mirrored in the heat rejection relationships.

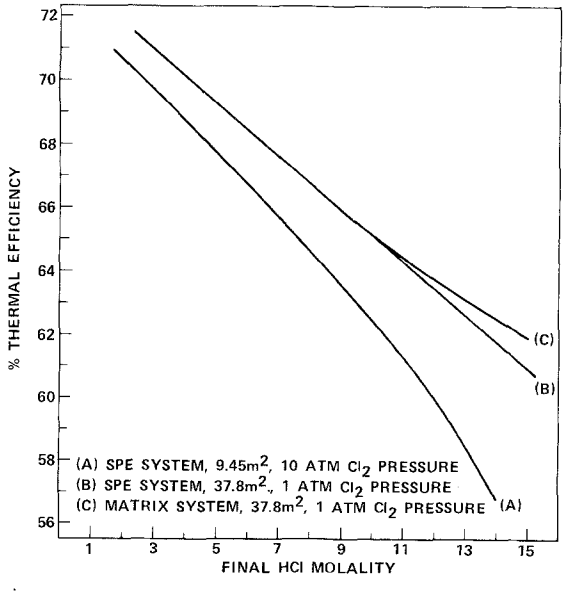

Fig. 8. Thermal efficiency in the H_2/Cl_2 systems.

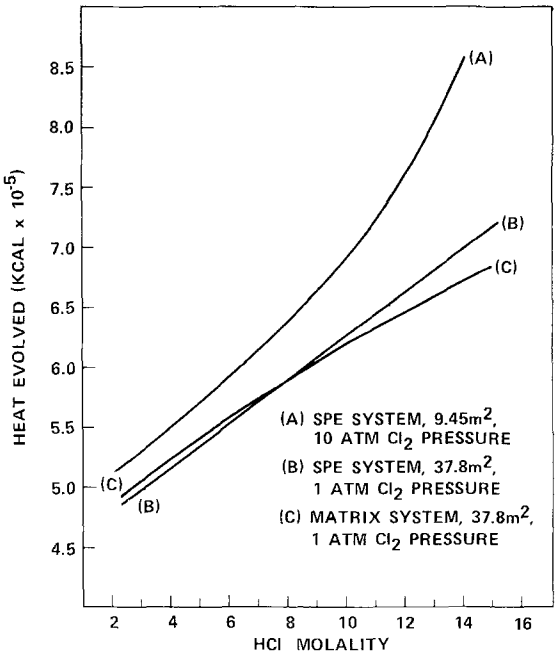

Fig. 9. Waste heat evolution in the H_2/Cl_2 systems.

4. The H_2/Br_2 systems

Solid polymer electrolyte and matrix systems were each considered at cell areas of 9.45 m^2 and 37.8 m^2 for the H_2/Br_2 couple. These areas correspond to approximately 100 mA cm^{-2} and 25 mA cm^{-2} respectively.

Fig. 10 follows several cell parameters in the 9.45 m^2 solid polymer electrolyte system over an acid concentration cycle which takes the final HBr molality near saturation. In contrast to the H_2/Cl_2 solid polymer electrolyte system, the HBr system exhibits only a modest increase in internal losses as the system approaches saturation. This arises because of the lesser solubility of HBr in water; the solubility limit being approximately 11.5 molal [16]. This limit precludes the system attaining a concentration sufficient to dehydrate the membrane to a point of high resistance. At 11.5 molal HBr concentration and 25° C, the vapour pressure of water over the acid solution is 8.2 torr; the vapour pressure of water over an 11.5 molal solution of HCl at the same temperature is 8.1 torr [4]. The model assumption of similar membrane resistance appears reasonable.

Fig. 11 is the equivalent plot for the HBr matrix system of the same area, operating over the same concentration range. The separator resistance

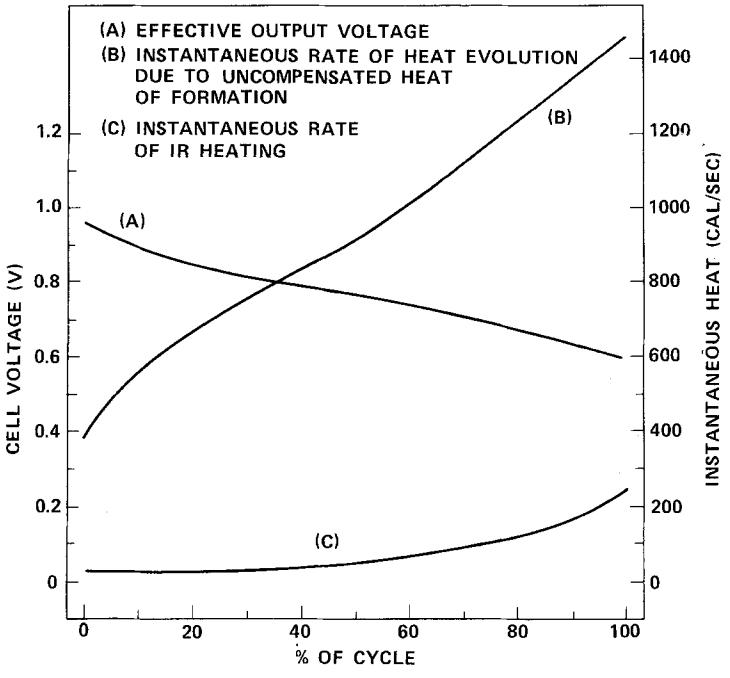

Fig. 10. Cell behaviour during the discharge of the 9.45 m² SPE systems; 10.1 molal final HBr molality.

here also exerts only a small influence over the system energetics. Fig. 12 presents the relationship between the H_2/Br_2 thermal efficiency and the final acid concentration for each case considered. The marked similarity at each cell area is due to the similarity in average separator resistance over the concentration cycle. The plots of Fig. 13, the system heat rejection as a function of final acid concentration, exhibit a similar congruence.

5. The H_2/I_2 systems

The low reversible cell potential of the H_2/I_2 couple requires battery currents considerably

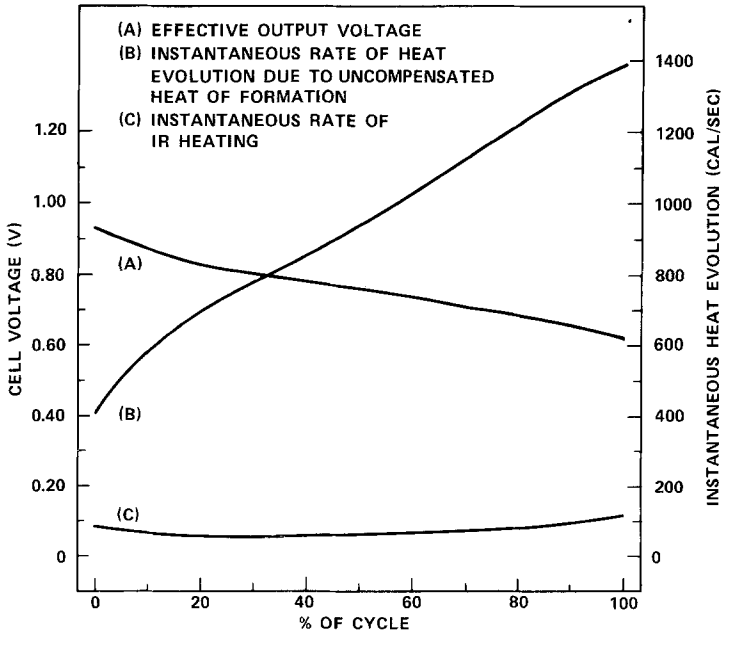

Fig. 11. Cell behaviour during discharge of the 9.45 m² matrix system; 10.2 molal final HBr concentration.

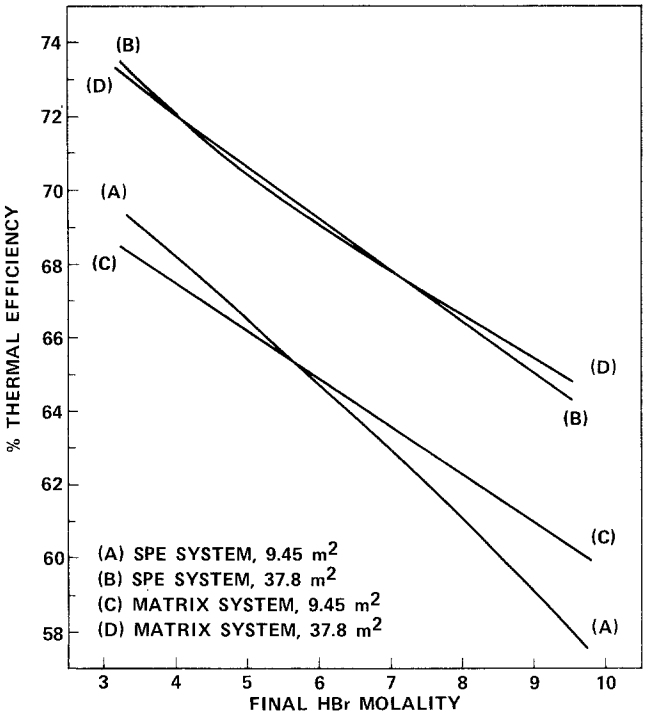

Fig. 12. Thermal efficiency in the H_2/Br_2 systems.

greater than those needed with the other two halogens. The hydriodic acid system is thus much more sensitive to separator resistance effects than the systems described above. For example, the H_2/I_2 matrix system of 9.45 m^2 cannot produce the prescribed output power at the start of the cycle; a solid polymer electrolyte system of the same area can operate only over the narrow range

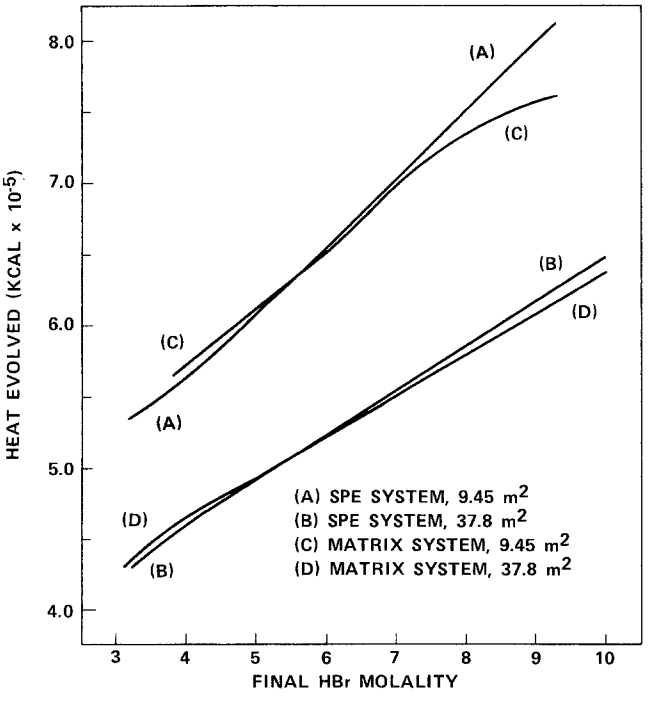

Fig. 13. Waste heat evolution in the H_2/Br_2 systems.

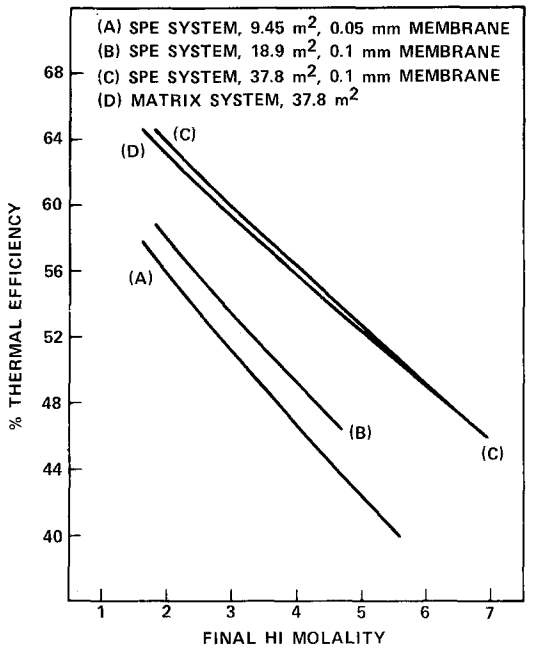

Fig. 14. Thermal efficiency in the H_2/I_2 systems.

of 1.4–2.3 molal HI. For these reasons, the high-current-density cases considered with the H_2/I_2 couple differed from those modelled with the lighter halogens.

The 9.45 m^2 system simulated employed a Nafion 1200 membrane of 0.05 mm thickness. While this is a commercially available material, its fragility makes its use in a large system troublesome. The second high-current-density system was a solid polymer electrolyte system of 18.9 m^2 which used a 0.1 mm membrane. A matrix system and a solid polymer electrolyte system of 37.9 m^2 were used as low-current-density cases.

Fig. 14 shows the thermal efficiency of each of these batteries as a function of the final HI molality. The efficiency in all cases is considerably less than that of the lighter halogens, a consequence of the higher current density and its attendant larger internal losses. These losses combine with the greater heat evolution per unit of electrical output (Fig. 3) to produce the heat rejection curves of Fig. 15.

6. Comparison of the three halogen systems

The thermal efficiency data of the three halogen systems are presented in Fig. 16 as a function of the corresponding fuel mass (water, hydrogen, and halogen). The heat rejected by each hydrogen–halogen couple is plotted versus the same variable in Fig. 17. There is a marked similarity among the curves which describe the H_2/Cl_2 and H_2/Br_2 systems. Despite the greater mass of bromine, water comprises over half of the fuel mass even at saturation. This mitigates the effect of the higher molecular weight of bromine to some extent. With these similarities in system performance, there are several aspects of a hydrogen–bromine

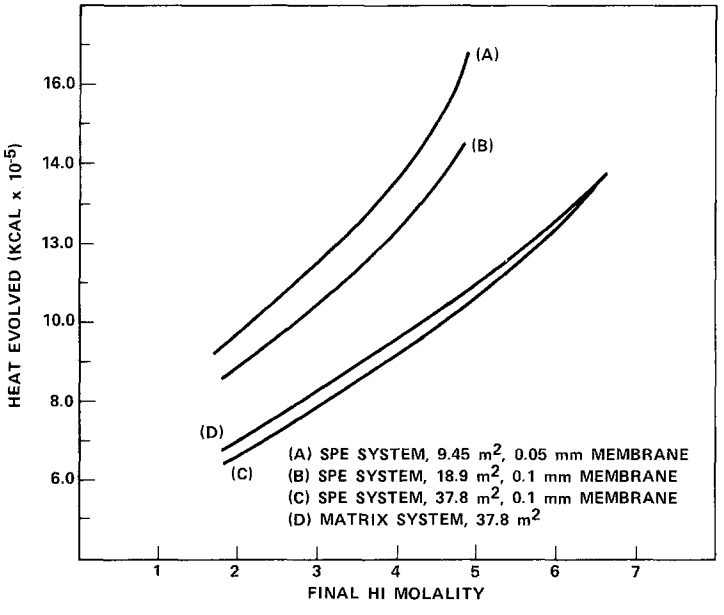

Fig. 15. Waste heat evolution in the H_2/I_2 systems.

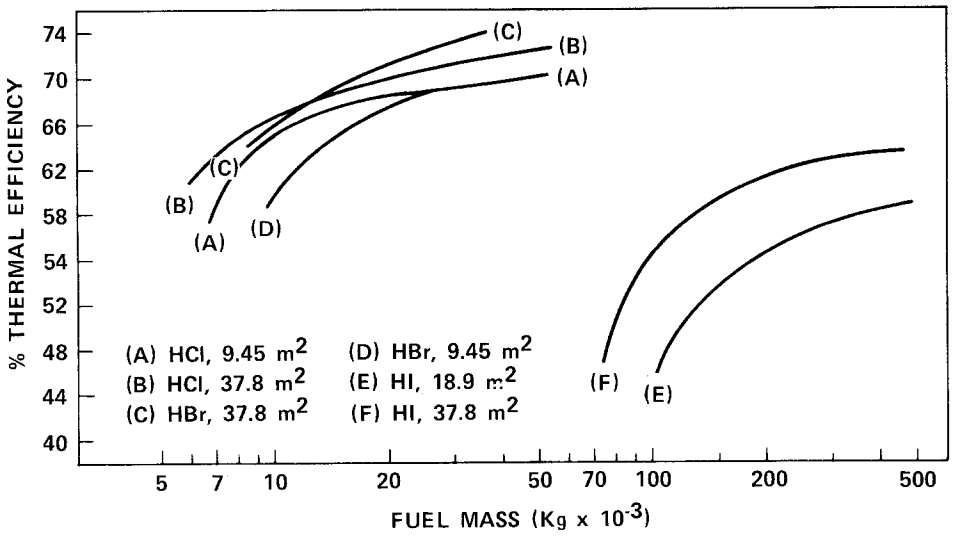

Fig. 16. Thermal efficiencies of the SPE systems using 0.1 mm membranes.

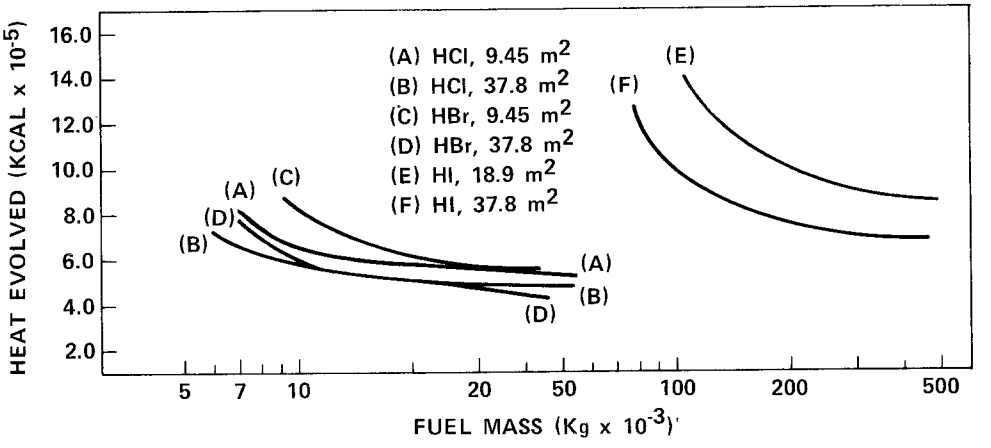

Fig. 17. Waste heat evolution of the SPE systems using 0.1 mm membranes.

system which might dictate its choice in an energy storage system. The liquid state of bromine at normal pressure and temperature simplifies fuel storage. The lower reversible potential of the bromine/bromide ion couple could eliminate system inefficiencies due to oxygen evolution during battery recharge. These benefits do come at the cost of materials problems, particularly where carbon or graphite materials are used.

The hydrogen–iodine system would appear to have little merit in an electrically recharged storage system. The appropriate application for the H_2/I_2 systems would lie where the recharge cycle exploits an energy source difficult to use with the lighter halogens, such as a direct solar regeneration.

Acknowledgement

The author wishes to thank the General Electric Company for its support in the completion of this work.

References

[1] J. McBreen *et al.*, Brookhaven National Laboratory Report #50924 UC94c, Upton, New York, USA (1978).

[2] M. Spaziante *et al.*, Brookhaven National Laboratory Report #25212, Upton, New York, USA (1978).

[3] J. F. McElroy, Paper presented at the DOE Chemical Energy Storage and Hydrogen Energy Systems Contracts Review, Hunt Valley, Maryland,

USA (1977).
[4] E. W. Washburn (editor), 'International Critical Tables', Vol. 3, McGraw-Hill, New York (1928).
[5] G. Akerloff and J. W. Teare, *J. Amer. Chem. Soc.* **59** (1937) 1855.
[6] H. S. Harned, A. S. Keston and J. G. Donelson, *ibid* **58** (1936) 989.
[7] W. J. Biermann and R. S. Yamasaki, *ibid* **77** (1955) 214.
[8] S. J. Bates and H. D. Kirschman, *ibid* **41** (1919) 1991.
[9] H. S. Harned and R. A. Robinson, *Trans Faraday Soc.* **37** (1941) 302.
[10] D. D. Wagman *et al.*, 'Selected Values of Chemical Thermodynamic Properties', NBS Technical Note 270-3, US Government Printing Office, Washington, D.C. (1968).
[11] J. J. Janssen *et al.*, *Electrochim. Acta* **22** (1977) 1093.
[12] E. N. Balko, S. D. Argade and J. S. Shrewsburg, US Patent 4 126 535.
[13] E. N. Balko *et al.*, US Patent 4 126 536.
[14] W. J. Hamer and H. J. DeWane, 'Electrolytic Conductance and the Conductances of Halogen Acids in Water', NSRDS-NBS 33, US Government Printing Office, Washington, D.C. (1970).
[15] M. S. Sherril and E. F. Izard, *J. Amer. Chem. Soc.* **81** (1959) 1280.
[16] W. M. Latimer and J. H. Hilderbrand, 'Reference Book of Inorganic Chemistry', Macmillan, New York (1951).